

Discrete Element Method (DEM) Simulation and Processing of Mo/Al₂O₃ Granules in a Fluidizing Bed

CHING-JANG LIN^{*}, WEN-CHENG J. WEI^{*,†}, TAKASHI IWAI^{**}, CHU-WAN HONG^{**}, AND
PETER GREIL^{**}

^{*}Institute of Materials Science and Engineering
National Taiwan University
Taipei, Taiwan, R.O.C.

^{**}Institute of Materials Science
University of Erlangen-Nuremberg
Erlangen, Germany

ABSTRACT

Fine Al₂O₃ particles are likely to form granules in a fluidizing reactor due to the interaction of several acting forces. The discrete element method (DEM) was employed to simulate the particle interactions in a fluidizing bed. The simulation results reveal that the granules floated and collided with the boundary walls or each other. The breakdown of soft granules under specified impingement angles and velocities is presented in order to reveal the fundamentals governing the adhesive strength of the granules. The criteria obtained from the simulation are compared with experimental results of studies on adhesive strength and the microstructures of four granules with various densities. The adhesive strength of granules was measured by means of a materials testing system (MTS). The detailed microstructures of the Mo/Al₂O₃ composite powders were analyzed by using SEM/TEM/EPMA techniques. The morphologies show that the Mo-species diffused into sub-micron capillaries in the granules during the MOCVD fluidization process and appeared in concentrations as high as 24 wt% in Al₂O₃ granules.

Key Words: DEM simulation, nano-composite, MOCVD, fluidizing bed, alumina, molybdenum

I. Introduction

Ceramic composites with nano-sized second-phase inclusion are reported to have good mechanical properties and can be made reliable with the help of microstructural modifications which reduce the inherent flow size (Niihara, 1991; Kinemuchi *et al.*, 1996). The fine inclusion can be produced from various sources. One of the reaction routes in the powder processing field of nano-structured ceramics, a metalorganic chemical vapor deposition (MOCVD), has been used, and it apparently offers a way to obtain nanometric dispersoid or homogeneous coating on submicron ceramic powders (Lin *et al.*, 2000). The surface forces of fine particles play a vital role in aerosol ceramic powder processes.

A nanocomposite is defined as a material of more than one Gibbsian solid phase with dimensions measured in the nanometric scale (Roy *et al.*, 1986). Alumina is usually selected as a model system. Molybdenum, due to its electrical conductivity, TEC mismatch, melting point, and Young's modulus, is the optimal choice for producing metal/Al₂O₃ composites if it is used under stringent conditions. Several Mo reinforced ceramic composites have

been studied and reported in the literature (Nawa *et al.*, 1994a, 1994b; Wei *et al.*, 1998; Wang and Wei, 1998), and significant improvement in the fracture strength and toughness of fine Mo/Al₂O₃ mixtures was recently proven by Nawa *et al.* (1994a) and Wang and Wei (1998). However, these hot-pressed composites are difficult to fabricate. The segregation and growth of the second-phase inclusion are the major obstacles yet to be overcome.

Geldart (1973) has studied the powder in a fluidizing bed and specified the key factors involved in the process. The finest ($\leq 20 \mu\text{m}$) powder exhibits high cohesiveness and, among the four groups of powders, is the most difficult to fluidize in a reactor (Kwauk, 1992). However, the fluidization behavior of the fine powder still can be described by a minimal fluidizing velocity (U_{mf}), (Wen and Yu, 1966), which can be expressed by the following equation:

$$U_{mf} = \frac{1}{1650\mu} d_p^2 (\rho_p - \rho_g), \quad (1)$$

where d_p is the mean particle size, ρ_p and ρ_g are the density of the particle and gas phase, respectively, and μ is the

[†] To whom all correspondence should be addressed.

viscosity of the flow. In addition, U_{mf} can be determined through measurement of the pressure drop in a fluidizing powder bed and is a function of the mean particle size and the average density of the particles.

Mo can be obtained from gas sources, such as Mo(CO)₆. The MOCVD process and properties of the (Mo, Cr) oxycarbides on various substrates, e.g., stainless steel and SiC, have been reviewed in previous works (Lo and Wei, 1997; Wei and Lo, 1998). The results show that the coating phase of molybdenum carbonyl is Mo₂O_xC_y in a crystalline structure similar to that of Mo₂C, but that the composition and crystalline structure may vary with the deposition conditions, e.g., temperature and pressure. This work focuses on the particle-particle interaction dynamics in an attempt to understand the microscopic motion of each particle in various granules in a fluidizing bed. In this study, different competitive interaction forces were incorporated in the simulation program. The discrete element method (DEM) was applied in order to analyze the particle-particle interactions of an aerosol system in a fluidizing powder bed and to clarify the granule disintegration dynamics. Special emphasis is placed here on the characteristics and microstructures of nano-Mo/Al₂O₃ granules after fluidizing in a powder bed is conducted by means of MOCVD processing, so that deposition of the Mo species in the Al₂O₃ can be resolved.

II. DEM Simulation of Particle-Particle Interaction Dynamics

Cundall originally developed DEM in 1971 to study rock mechanical and granular medium problems (Cundall, 1971; Cundall and Strack, 1979). Recently, Tsuji *et al.* (1993, 1994) and Bortzmeyer (1997) used Cundall's DEM method to simulate various particle motions in a fluidizing bed or attrition mill. Contact forces between particles were modeled, and the forces were expressed through the use of a spring, dash-pot and friction slider. Particle segregation and attraction were reported, and the latter was strongly related to the plasticity of the contacts and to the Young's modulus of the granules. This produced either soft or hard granules, which were categorized according to the Young's modulus into two groups: less than 30 MPa or greater than 3000 MPa. Free rotation of the particles was present in soft granules, but not in hard granules.

Horn (1990) pointed out that the surface forces between two bodies had their origins in the interatomic forces acting between all of the atoms of those bodies, as well as between the atoms of any interfering medium. A recent application of simulation in a colloidal system was presented by Hong (1996, 1997, 1998). Since all known particle-particle interaction forces were integrated in one model, the features of three dimensional particle-packing

could be resolved. His work successfully interpreted these phenomena in the pressure filtration and centrifugal casting of ceramic slurries.

In aerosol processing, the particles are suspended in gas. The attraction forces existing in an aerosol system include electrostatic surface charges and capillary forces, which are both strongly affected by humidity. Water will condense on the small meniscus between two particles in an atmosphere with high humidity, causing bridging and charging of the powder (Horn, 1990). The van der Waals (vdW) force is normally weaker than the electrostatic and capillary forces. However, the van der Waals attractive force remains an important factor for the formation of agglomerates in aerosol systems without humidity.

Based on studies by Hamaker, the van der Waals interaction free energy, V_{vdW} , between two spheres of different sizes can be expressed as (Hong, 1997)

$$V_{vdW} = -\frac{A_H}{6} \left[\frac{2r_1r_2}{h^2 + 2h(r_1 + r_2)} + \frac{2r_1r_2}{h^2 + 2h(r_1 + r_2) + 4r_1r_2} + \ln \frac{h^2 + 2h(r_1 + r_2)}{h^2 + 2h(r_1 + r_2) + 4r_1r_2} \right], \quad (2)$$

where A_H is the Hamaker constant, r_1 and r_2 are the radii of the spherical particles, and h is the surface-to-surface distance. For fine ceramic powders, the van der Waals attractive force dominates at interface distances less than 10 nm. According to Eq. (2), the van der Waals interaction force can lead to the following form (Hunter, 1987):

$$\bar{F}_{vdW} = -\frac{\partial V_{vdW}}{\partial h} = -\frac{A_H}{6h^2} \left(\frac{r_1r_2}{r_1 + r_2} \right), \text{ when } r_1, r_2 \gg h. \quad (3)$$

The van der Waals interaction force is proportional to the Hamaker constant and is a function of the particle size and surface distance. The Hamaker constants of Al₂O₃ have been previously determined to be 15×10^{-20} J, 5.2×10^{-20} J, and 3.6×10^{-20} J in vacuum (air), water, and n-dodecane, respectively (Bergstroem *et al.*, 1996).

The relative significance of the interaction forces, such as electrical forces, the van der Waals attractive force, Brownian force, Stokes viscous force, gravitational force, and internal force exerted between suspending colloids in aqueous or aerosol systems, are summarized in Table 1. First of all, the van der Waals attractive force is an important factor in fine particle agglomeration in a dry aerosol system. In addition, mechanical forces, such as viscous, gravitational, buoyancy, hydrodynamic, inertial, and contact kinetic forces, become important in situations where electrostatic stabilization is not effective. There-

Table 1. Main Differences in Characteristic Forces between Colloids in Aqueous (Hong, 1997) or Aerosol Powder Systems

Characteristic Force	Aqueous system	Aerosol system
Electrical force $f(r, h, \epsilon\epsilon_0\zeta)$	$\zeta = 50 \text{ mV}^*$ dominant force	$\zeta = 0 \text{ mV}$
vdW attractive force $f(r, h, A_H)$	$A_H = 4.76 \times 10^{-20} \text{ J}$	$A_H = 15 \times 10^{-20} \text{ J}^*$ dominant force
Stokes viscous force $\bar{F}_d = -6\pi\eta r\bar{v}$	$\eta = 10^{-3} \text{ kg/ms}$	$\eta = 10^{-7} \text{ kg/ms}$
Buoyancy force $\bar{F}_b = -(4/3)\pi r^3 \rho_f \bar{g}$	$\rho_f = 1000 \text{ kg/m}^3$	$\rho_f = 0.6 \text{ kg/m}^3$
Gravitational force $\bar{F}_g = (4/3)\pi r^3 \rho_p \bar{g}$	$\rho_p = 3980 \text{ kg/m}^3$	$\rho_p = 3980 \text{ kg/m}^3$
Rotational resistance (Inertial force), $\bar{M}_r = -8\pi\eta r^2 \bar{\omega}$	$\eta = 10^{-3} \text{ kg/ms}$	$\eta = 10^{-7} \text{ kg/ms}$
Hydrodynamic lift $\bar{F}_h = \pi r^3 \rho_g \bar{\omega} \times \bar{v}$	$v = 0.01 \text{ m/s}$	$v = 0.001 - 1.0 \text{ m/s}$

*Dominant force in each system.

fore, all of these contributions to the force between two particles depend not on the centers of the particles, but on the distance between their surfaces (Horn, 1990). Thus, the surface distance is defined as the nearest surface-to-surface distance between two particles.

The DEM uses Newton's second law to describe particle motion. The interactions are formulated as functions of forces and momentums. Pair-interaction laws are used in this work, but not multi-body interaction laws. The multi-body interactions can be resolved through the summation of all pair interactions. The constituent equation for the particle-particle interaction force can be expressed as (Hong, 1997)

$$\bar{F}_p = \frac{-\partial V_{total}}{\partial h}, \quad (4)$$

$$V_{total} = V_{vdw} + V_{el}. \quad (5)$$

According to Newton's second law, the motion equations can be shown as follows:

$$\sum \bar{F}_i = \sum \bar{F}_{pi} + \bar{F}_d + \bar{F}_g + \bar{F}_b + \bar{F}_h + \sum \bar{F}_{ni} = m\bar{a}, \quad (6)$$

$$\sum \bar{M}_i = \bar{M}_r + r\sum \bar{F}_{ti} = J\dot{\bar{\omega}}, \quad (7)$$

where \bar{a} and $\dot{\bar{\omega}}$ are the linear and angular acceleration, respectively, m is the mass of the particle, and J is the mass moment of inertia.

At time t , the unbalanced forces ($\sum F_i \neq 0$) and moments ($\sum M_i \neq 0$) produce particle linear (a) and angular ($\dot{\omega}$) accelerations. At time $t + \Delta t$, these coordinates can be used to compute the new displacements at the end of the current time increment. The process is repeated until the

unbalanced forces and momentums approach equilibrium or until the process is stopped. In the case of an aerosol system, $\sum F_i = \sum M_i = 0$ should apply for every particle in static equilibrium.

III. Experimental Procedure

1. Materials and Processing

The mean size of alumina raw powder (AKP-50, Sumitomo Chemical Co., Tokyo, Japan) is $0.3 \mu\text{m}$. Four types of alumina granules were prepared, either with 43% theoretical density (% T.D.) obtained by screening between $-100/+140$ mesh sieves, 49% T.D. obtained by spray drying, 54% T.D. obtained by slip casting, or 61% T.D. obtained by calcination at 1000°C . The last two granules were crushed and then screened between $-100/+140$ mesh sieves.

The fluidization and MOCVD processes were reported in a previous work (Lin *et al.*, 2000). Molybdenum hexacarbonyl ($\text{Mo}(\text{CO})_6$, Alfa Chemicals Co., Newburyport, MA, U.S.A.) was put in a source chamber and carried by N_2 gas (99.9% pure) at a flow rate of 0.5 to 5.0 l/min. According to Lander's results (Lander and Germer, 1947), the saturation pressure P of the Mo-carbonyl is 10.7 torr at 80°C . The source chamber was maintained at constant pressure and temperature, 80°C , by means of a water bath. The coating temperature was kept at 325°C . In this study, the gas flowed upward through a powder bed. An established method (Cheremisinoff and Cheremisinoff, 1986) was used to observe the pressure drop at various flow velocities and to determine the U_{mf} .

2. DEM Simulation Conditions

Table 2 shows the conditions selected for the DEM simulation used for aerosol fluidizing bed processing. The five sizes of Al_2O_3 particles appeared in a normal distribution. Two-dimensional and three-dimensional simulations were conducted and the results compared. The granule sizes were set from 10 to $2.5 \mu\text{m}$. The collision velocity and impingement angle of the granules ranged from 0.1 to

Table 2. The Conditions Selected for DEM Simulation in this Study

Material	Alumina	
Particle size distribution	0.1 ~ $0.5 \mu\text{m}$, normal distribution	
Dimension	2-D	3-D
Size of granule (μm)	10 or 5	5 or 2.5
Solid loading	43, 49, 54, 61% T.D.	
Collision velocity (cm/sec)	0.1, 0.5, 1, 2, 5, 7, 10, 20, 50, 70, or 100	1, 5, or 10
Collision angle (degree)	5, 10, 20, 30, 45, or 80	

100 cm/sec and from 5° to 80°, respectively.

In the simulation system, various granules were created with relative densities of 43, 49, 54, or 61% T.D. in the 2-D simulation, and 43% T.D. in the 3-D simulation. For instance, Al₂O₃ granules were generated by random set generators to obtain a final granule diameter of 10 μm and a specified density, which would contain thousands of ultimate particles in 5 different sizes, with a mean size of 0.3 μm. For example, a 10 μm Al₂O₃ granule with 43% T.D. is shown in a rectangular area 12.0 μm × 24.0 μm (Fig. 4). Periodic vertical boundaries and a downward gravitation force were assumed.

The Reynolds number of the granules (*Re*) under fluidization conditions is less than 0.7 which indicates a laminar flow. Therefore, the Stokes viscous drag force is considered, but the long-range many-body hydrodynamic interactions are neglected due to the low Reynolds number.

In order to determine the size reduction after granule impingement against the boundary, the mean secondary granule size (\bar{d}) is defined as (German, 1994)

$$\bar{d} = \left[\frac{\sum n_i d_i^2}{\sum n_i} \right]^{1/2}, \quad (8)$$

where d_i is the average dimension (shortest and longest diameters) of the n_i secondary granule. The mean relative size (\bar{d}/d_0) of the granules was used to express the simulation results, where d_0 is the primary size of the granule.

3. Properties

Crystalline phases of deposited granules were identified by means of an X-ray diffractometer (XRD, PW1729, Philips Co., Eindhoven, the Netherlands). The composition profiles across the center of the granules were determined using an electron probe X-ray microanalyser (EPMA, JXA-8600, JEOL Co., Tokyo, Japan), which was operated at 15 keV with an electron probe size of 1 μm and a current of 1×10^{-7} A. The morphology and composition of the deposited powders were also analyzed using a TEM (100CXII, JEOL Co.) or an SEM (XL30, Philips Co.) equipped with an X-ray energy dispersive spectroscopy (EDS, DX-4, EDAX Co., Prairie View, IL, U.S.A.).

In order to ensure that the microstructure of a cross-section of the granule was free of artifacts, each specimen was prepared in the following manner. The deposited granules were mixed with Bakelite and then hot-mounted. The surface was ground with a 6 μm diamond medium and then polished using 60 nm silica colloids. Between each stage, the specimen was cleaned by means of ultrasonication in a water bath. The specimen was put in a dry oven at 105°C and left overnight. Dry N₂ gas was used to

blow clean the polished surface, which was then coated with a carbon film to prevent electron charging during SEM observation.

In order to estimate the granule strength, a compaction test similar to those reported previously (Matsumoto, 1986; Walker and Reed, 1999) was executed. The test was carried out by filling a double action steel die with 10 grams of granules with specific relative densities, followed by uniaxial compression at a rate of 10 N/sec using a universal machine (MTS 810, MTS Co., Canton, MA, U.S.A.). The load and displacement were recorded automatically.

IV. Results

1. Fluidization Behavior

Due to the van der Waals attractive force, alumina fine powder tends to agglomerate in an aerosol powder bed. The relationship between the pressure drop and flow velocity is determined through experimentation, and a minimal fluidization velocity (U_{mf}) can, thus, be determined. The pressure drop of the bed, ΔP_B , initially rises as the gas velocity, U , increases. The results for ΔP_B vs U are shown in Fig. 1. At the time when the bed begins to fluidize at the initial stage, the superficial velocity is known as the minimal fluidizing velocity, U_{mf} . Experimental results show that the U_{mf} of AKP-50 dry powder is far greater than the U_{mf} of a powder with a particle size of 0.3 μm. In fact, the measured U_{mf} of the AKP-50 powder is between the values of two hard granules with 61% T.D. and mean sizes of 100 μm and 150 μm. Additional experimental results show that the U_{mf} of the finer (–400 mesh)

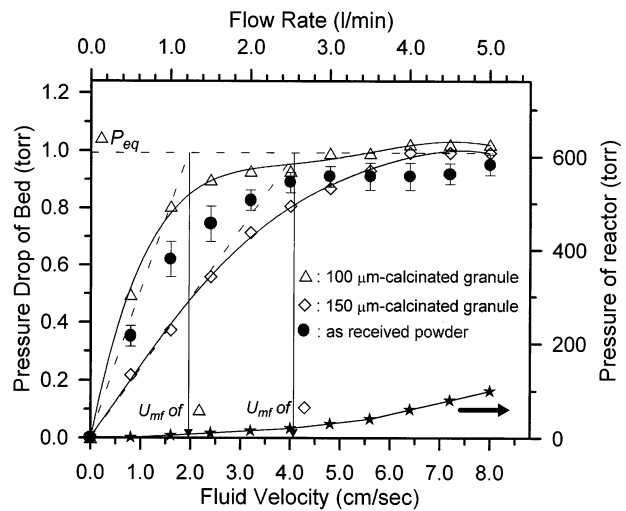


Fig. 1. Minimal fluidizing velocity, U_{mf} , of calcinated alumina granules with diameters of 100 μm and 150 μm, and as received AKP-50 powder. The mass of each batch was kept at 25 gm.

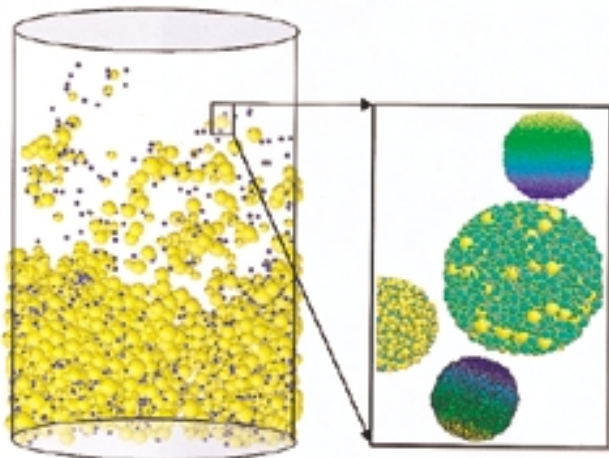


Fig. 2. A 3-D schematic diagram showing granules containing submicron particles in a fluidizing bed.

and coarser (-100/+140 mesh) agglomerates of the AKP-50 powders prepared by means of granulation are not significantly different from the as-received powder. The results show that the fluidization behavior of alumina powder in various granulating conditions is similar due to the high cohesiveness of the fine powder during fluidization. Consequently, a greater velocity is required to initialize fluidization of the fine powder.

2. Simulation Result

The 3-D schematic diagram illustrates the granules of submicron-powder in a fluidizing bed, as shown in Fig. 2. The gas flow uniformly passes through the distributor, and fine powder tends to granulate and fluidize in the bed. The granules collide with each other or the walls of the reactor at different speeds and impingement angles.

The simulation work generated 2-D and 3-D granules with different packing densities. Figure 3 shows the packing structure of granules with a packing density in-

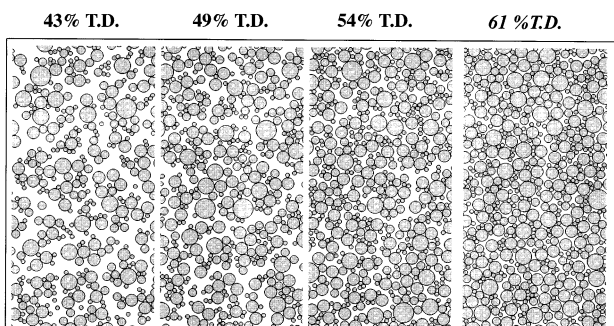


Fig. 3. The various packing structures of granules with specific relative densities generated by a random setter.

creasing from 43 to 61% T.D. It is noted that the surface distance and pore size are closely related to the relative density.

Figure 4 shows one typical evolution of the structure breakdown of a 10 μm granule with 43% T.D. at 4 time intervals. The velocity and impingement angle of the granules were fixed at 10 cm/sec and 10°. The DEM simulation shows that all the particles in a granule appear to have the same velocity due to the gas flow at an initial

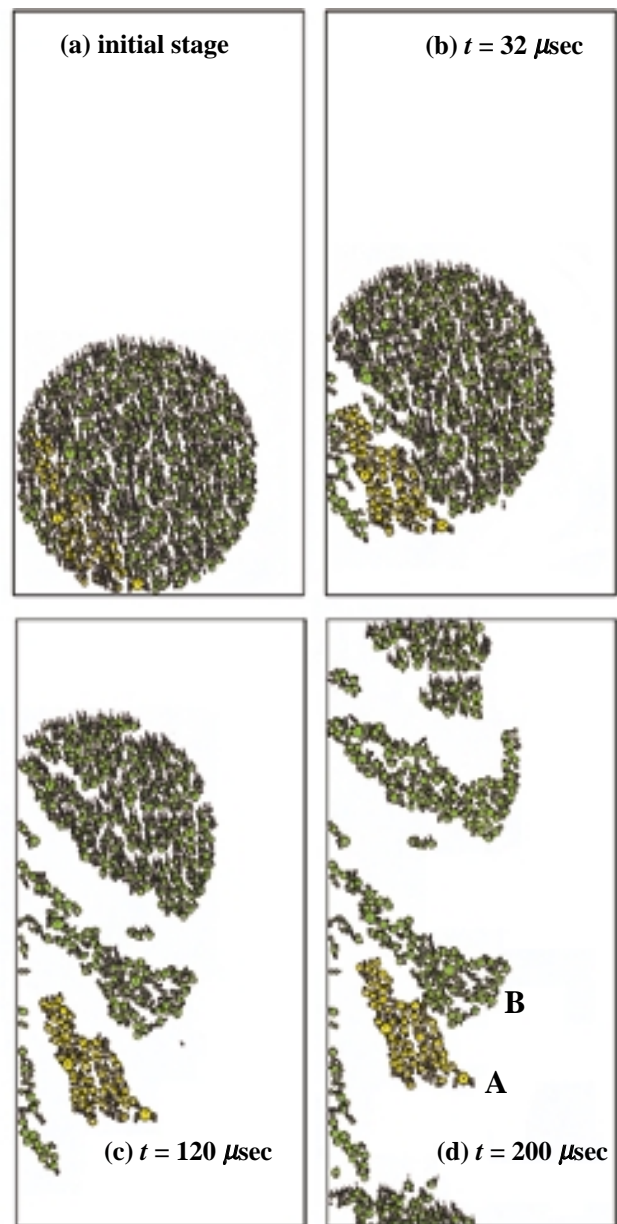


Fig. 4. Evolution of the breakdown structure of a 10 μm alumina granule with 43% T.D. impinging against a boundary at an angle of 10° and a velocity of 10 cm/s. The small trajectory on each particle is the velocity vector.

stage (note the vectors in Fig. 4(a)). The granule breaks due to collisions with the left-hand boundary. In the initial stage of collision with the boundary, the normal force causes deformation and creates microcracks along the specific (30° to 45°) direction of the granule. When the kinetic forces of a contact overcome the attractive force, a group of particles or secondary granules separates from the primary granule. Furthermore, the tangential force causes disintegration, resulting in the separation of small debris from the primary granule along micro-cracks. Some debris rotates due to the hydrodynamic lift and frictional drag from the boundary and medium. The simulation results show another interesting phenomenon: the re-association of particles. The secondary granules A and B, indicated in Fig. 4(c) and (d), form a new granule at later stages.

The mean relative size (\bar{d}/d_0) of the secondary granules was calculated according to Eq. (8) and is shown in Fig. 5. The size decreases when the collision velocity increases. The critical disintegration collision velocity (V_c) is dependent on the packing density of the granules. V_c is 2, 5 or 10 cm/sec for soft granules of 43, 49 or 54% T.D., respectively. Note that the hard granule of 61% T.D. cannot be disintegrated when the collision velocity is below 100 cm/sec. It appears that smaller secondary granules are easier to obtain under a velocity higher than the critical disintegration velocity. The mean relative size (\bar{d}/d_0) of secondary granules is reduced to 0.2 at most (mean aspect ratio ~ 2.0). Therefore, the secondary granules round up again due to re-association in fluidization.

The disintegration results of the 3-D simulation are similar to the 2-D results with the exception that the mean relative size of secondary granules in the 3-D simulation is larger than that in the 2-D simulation. It is also noted that

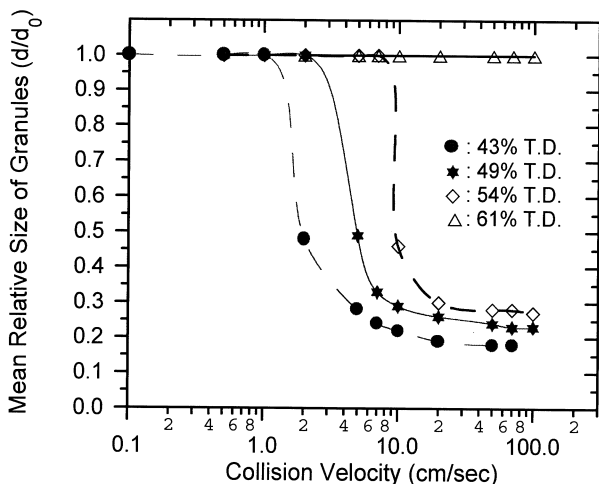


Fig. 5. The mean relative size of specific granules under various collision velocities. The impingement angle was fixed at 10°.

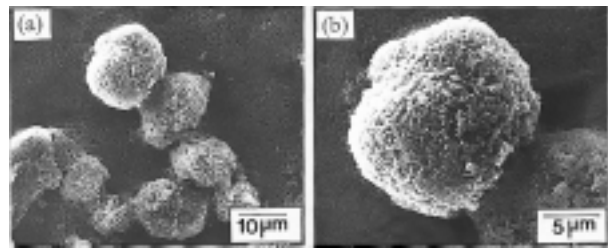


Fig. 6. SEM micrographs, at two levels of magnification, of Mo-species/alumina granules with 54% T.D. prepared using MOCVD in a fluidizing bed at 325°C for 1 h.

the mean coordination number in a 3-D granule is larger than that of particles in a 2-D granule. This means that higher coordination numbers lead to a larger adhesive area and attractive force.

3. Characterization of Deposited Powder

Figure 6 shows SEM micrographs revealing the surface morphologies of Mo-species/alumina granules with 54% T.D. prepared using MOCVD in a fluidizing bed at 325°C for 1 h. The surface morphology appears to be equiaxial in shape and reveals the porous structure of deposited granules. The Mo-species is not visible at low magnification. The other observations show the size of the granules ranging from 10 to 100 μm .

A TEM image of a few Mo-species/Al₂O₃ particles with 43% T.D., prepared using MOCVD in a fluidizing bed at 325°C for 1 h, is shown in Fig. 7. The particles were supported on a perforated carbon film for observation. The features of the individual particles show that the distance between the surfaces of the Al₂O₃ particles is about 5 nm. Some Al₂O₃ particles covered with amorphous film of Mo-species are darker in contrast to others due to atomic absorption by the deposited species to the electron beam.

Figure 8(a) shows a cross-section of a few Mo-species/alumina granules with 54% T.D. prepared using MOCVD in a fluidizing bed at 325°C for 1 h. Figure 8(b) shows the corresponding X-ray intensity mapping of a Mo element in the same region as in Fig. 8(a). The Mo-species deposited in the alumina granules is evident, but the concentrations vary slightly from the surface to the center of the granules. A higher magnification of one granule is shown in Fig. 8(c). In this figure, it appears that the cross sections of these granules are free from polishing artifacts, such as grinding medium contamination. The mean particle size of the alumina is close to 0.3 μm , and the particles are in slight contact with each other. The cross section of the granule remains porous due to the relative density (54%) of the granule.

The deposited granules were characterized by means

of semi-quantitative analysis using SEM-EDS and XRD analysis. The EDS spectrum of the deposited powder shows a concentration of Mo within the alumina powder, and the Mo-species content increases as the deposition time increases. In order to confirm the structure of the Mo-species, composite powders deposited at different temperatures were analyzed by means of XRD, and the results show a broadened XRD peak at 22° to 30° (2θ angle), implying that the Mo-species is in an amorphous phase.

Quantitative and elemental distributions of the cross-section of the deposited granules with various densities and Mo-species contents in Al_2O_3 granules at various depths relative to the surface were analyzed using EPMA equipped with a wave dispersive spectroscopy (WDS). The EPMA line scans of the Al and Mo elements show that the distribution of Mo-species is similar from the surface to the center in granules with 43% and 54% T.D.² The concentration of Mo in an Al_2O_3 granule is as high as 24 wt%.

Figure 9 shows the density of the various granules in response to compaction pressure. At low pressures, the relative density remains constant up to a break-point pressure, at which point the slope of the relative density with respect to the logarithmic pressure abruptly increases. The break-point pressure has been defined as the apparent yield pressure of the granules (Matsumoto, 1986). The apparent yield pressure is related to the strength of the individual granules. The yield pressure of the 43, 54, and 61% T.D. granules is 0.3, 0.56, and 2.25 MPa, respectively. Note that the yield pressure of the deposited granule of 54% T.D. increases from 0.56 to 0.91 MPa. This implies that the Mo-species deposited on Al_2O_3 granule supply additional adhesive force.

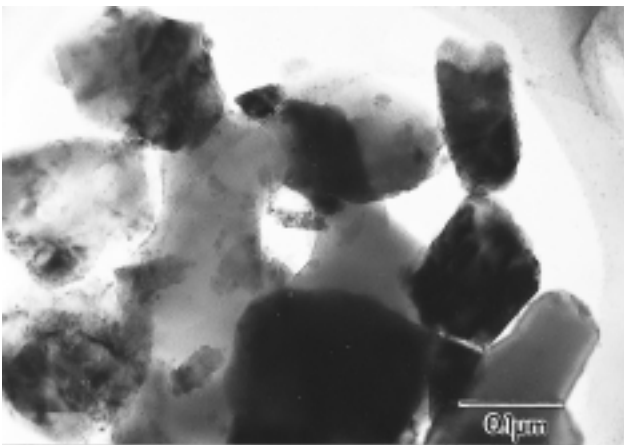


Fig. 7. TEM image of a few Mo-species/alumina particles prepared using MOCVD in a fluidizing bed at 325°C for 1 h.

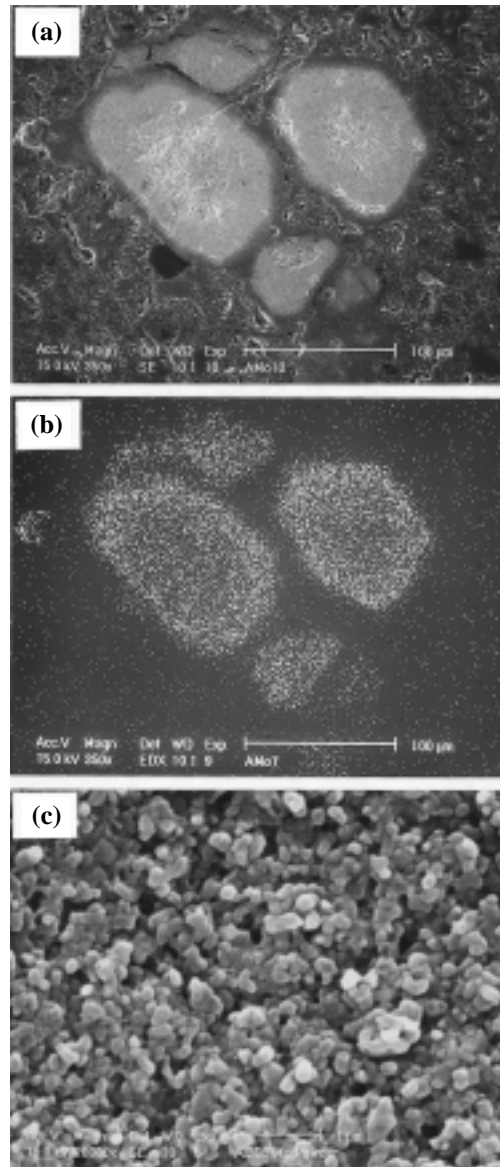


Fig. 8. (a) The cross-section morphology of Mo-species/alumina granules with 54% T.D. prepared using MOCVD in a fluidizing bed at 325°C for 1 h, (b) corresponding X-ray mapping of the Mo element, and (c) high magnification of the cross-section morphology.

V. Discussion

1. Granule Disintegration and Reassociation

According to the results of the experiment and simulation, the fine powder tends to agglomerate in an aerosol fluidizing bed. The soft granule can disintegrate during fluidization because the mechanical energy is greater than the attractive energy. Disintegration and reassociation of

² The analysis of Mo distribution will be presented in another report.

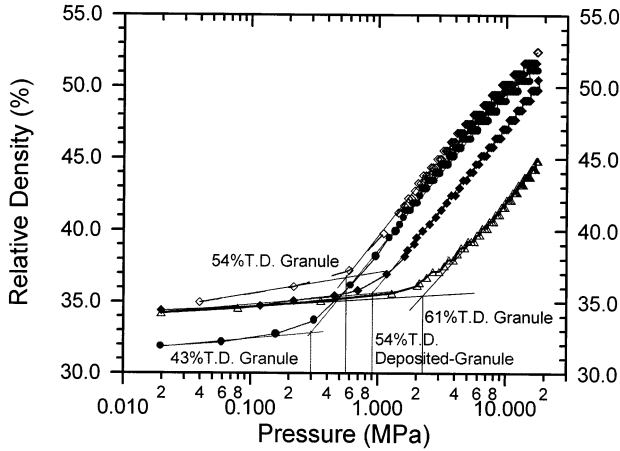


Fig. 9. Compaction results of granules of alumina with various packing densities depicting the apparent yield pressure of the granules.

the particles occurs during fluidization. The criteria for the disintegration and re-association of particles to form secondary granules must be determined in order if a fluidizing bed and MOCVD are to be used to obtain granules with homogeneous Mo-species.

From the microscopic viewpoint, the particle-particle interaction dynamics of submicron ceramic powders with granules in the fluidizing powder bed are visualized in Figs. 2 and 4. The deformation and breakdown structures under various collision angles (from 5 to 80°) were studied. The contact forces (F_n and F_t) between each pair of impinging particles and boundaries depend on the impingement angles and collision velocities. The results show that the deformation of the granule is due to the effects of the normal force (F_n) and the rigidity of the granule. On the other hand, the frictional drag force (F_d) is dependent on the magnitude of the effective normal force (F_n) and the friction coefficient (μ). When the tangential force F_t is less than μF_n , the normal force F_n causes slippage of the granule. When $F_t = \mu F_n$, relative sliding of the particles in a granule occurs. Due to the normal force of impingement, the resulting tangential force causes disintegration if $F_t > \mu F_n$, resulting in the separation of small debris from the primary granule. Generally, the tangential force dominates the initiation of granule disintegration and separation from the primary granule. The results appear to show that small secondary granules are easier to obtain at a velocity higher than the critical disintegration velocity. Moreover, the disintegration results of a series of 3-D simulations show that higher coordination numbers lead to a larger adhesive area and attractive force. It is believed that the disintegration behavior of ceramic granules is dependent on the granulation conditions.

The reason for the homogeneous deposition in soft alumina granules is two-fold. First, the MOCVD is the

gas reaction route. This process causes molecular diffusion of the Mo-species into submicron channels inside the granules. Second, is the disintegration and re-association of soft granules (density less than 54% T.D.) in a fluidizing bed. The particles from the soft granule disintegrate and may form secondary granules. That reduces the size of the granule and reduces the length of the diffusion path.

2. Granule Strength

The strength of packing particles is determined by the particle-particle interaction forces and packing structure (German, 1994; Walker and Reed, 1999). The fine particles can agglomerate due to the van der Waals attractive force and capillary forces if they are exposed to a humid atmosphere. When the humidity condenses on the necks of the particles, the capillary force should be taken into consideration. The condensation of water from humid vapor was controlled in this study, but it is difficult to totally rule out the effects of humidity. Therefore, the simulation also considered this possibility.

In addition to the van der Waals and capillary forces, the atomic bonding force of the necks introduced by calcination at 1000°C should be counted as part of the adhesive force. Meanwhile, the porosity, coordination number, and surface distance of the packing structure also influences the strength of the granule. German proposed that the strength of packing particles (σ_g) can be formulated as follows (German, 1994; Rietema, 1991):

$$\sigma_g = \left[\frac{6(1-\varepsilon)}{\pi} \right]^{2/3} \times \frac{N_c}{2} \times \frac{F_a}{d^2} = k \times f \times N_c \times \frac{F_a}{d^2}, \quad (9)$$

where ε is the porosity, N_c is the packing coordination, F_a is the adhesive force of the packing particle, d is the diameter of the particle, k is a shape factor, and $f(=1-\varepsilon)$ is the fractional density. In random packing, the coordination number varies according to the packing density as well as from particle to particle. Hence, only an average coordination number (N_c) can be assumed. It was suggested by Smith (Rietema, 1991) that the relationship between the coordination number and the porosity is given by $N_c \times \varepsilon = 3.1$. Therefore, the values of N_c of the granules in 43, 49, 54, and 61% T.D. are 5.4, 6.1, 6.7, and 7.9, respectively.

The value of the capillary force (F_c) follows the estimation (German, 1994):

$$F_c = 5\gamma d, \quad (10)$$

where γ is the surface energy and d is the particle size. When the saturation condition of second phase in granules is considered, Eq. (10) can be modified to obtain

$$F_c = 5S\gamma d, \quad (11)$$

where S is the degree of saturation (the fraction of the pore volume filled with second phase). The saturation of humidity and the ratio of atomic bonding of a granule calcinated at 1000°C, in the capillary area, are equal to 0.8% and 0.2%, respectively. The adsorption of humidity was taken from the mass loss (0.1 wt%) of as-received powder heated to 105°C for 12 h. The saturation of humidity is equal to 0.8 vol% of the pore volume. The saturation of atomic bonding was determined by taking the initial shrinkage value obtained from thermal mechanical analysis (TMA) at 1000°C. In addition, the surface energy (Kingery *et al.*, 1976) γ_{l-v} of H₂O is 72 ergs/cm², and γ_{s-s} of Al₂O₃ is 905 ergs/cm². The interface energy and saturation between Al₂O₃ and Mo-species are difficult to define since some degree of chemical and physical adsorption takes place (Szekely *et al.*, 1976). Therefore, the interface energy can be determined by referring to the Al₂O₃-silicate glaze (Kingery *et al.*, 1976) and assuming a value of 500 ergs/cm², with the saturation of Mo-species set at 0.2%.

In a random packing structure, the distance between neighboring particles is a normal distribution. Figure 10 shows the distance between neighboring particle-particle surfaces in granules with various densities estimated from the simulated microstructures as shown in Fig. 3. Based on the weakest-link theory (Papargyris, 1998; Lok and Lee, 1997), the statistical fraction of the particle connection providing the apparent strength of a loose-packed granule is about 0.16, which is the accumulation of the shorter surface distances.

The apparent distances under which the volumes of particles accumulate to 0.16 are 4.9, 4.2, 3.3, or 2.1 nm for granules with 43, 49, 54, or 61% T.D., respectively. The

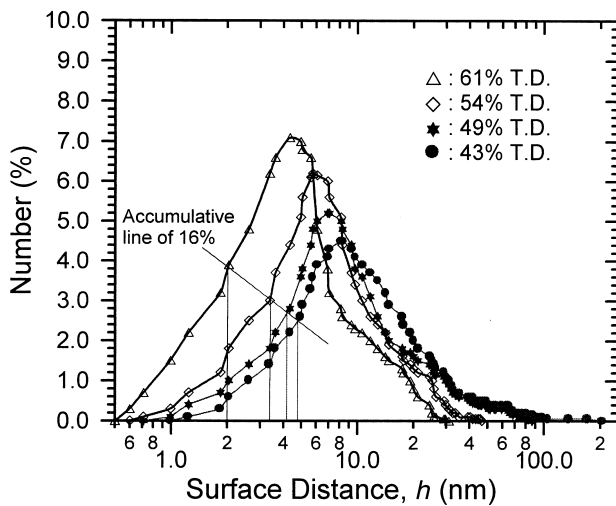


Fig. 10. The surface distance distributions of neighboring particles in granules with various densities. The values were estimated based on simulated granular structures in 2-D cases.

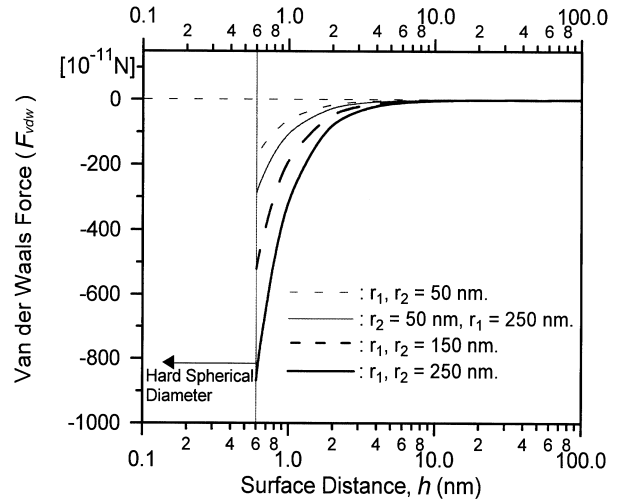


Fig. 11. Estimate of the van der Waals interaction forces versus the surface distance of particle interaction under various sizes (r_1, r_2). A definition of the hard spherical diameter was given by Hong (1997).

data also shows that looser particle packing results in a broader surface distance distribution.

The van der Waals interaction force versus the surface distances between neighboring particles with various particle sizes was calculated according to Eq. (3), and the results are shown in Fig. 11. The shortest surface distance between neighboring particles is limited by the hard spherical diameter of a molecule ($\sigma_{hd} \sim 0.6$ nm) (Hong, 1997). The results show that the attractive force increases as the surface distance decreases and particle size increases. Therefore, the strength (the ratio of force to surface area) becomes more significant for smaller particles. Generally speaking, shorter surface distances lead to greater van der Waals attractive forces.

From Eqs. (9) and (11), numerical calculation (Fig. 12) shows the estimated strength of various granules plotted against the surface distances between neighboring particles of sizes $d_1 = 100$ nm and $d_2 = 500$ nm. The strength of granules increases as the van der Waals force, capillary force, and atomic bonding come into play. The strength curves shown in Fig. 12 move downward as additional (capillary and bonding) forces are included in Eq. (9).

Four experimental yield strengths of various granules determined by means of compaction tests (Fig. 9) are also plotted in Fig. 12. The corresponding surface distance is between 0.9 nm to 2.1 nm. The range of the surface distance is slightly smaller than that from the corresponding simulation results, as shown by the marked region in the figure, with respect to the 43%, 54%, and 61% T.D. granules. The experimental results of the yield pressure of various granules are similar and consistent with the numerical calculation results.

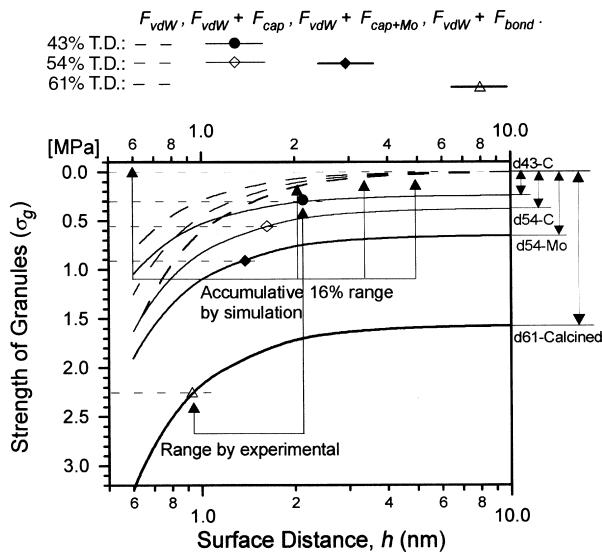


Fig. 12. Estimated strength of granules with various densities versus the surface distance between neighboring particles of sizes $d_1 = 100$ nm and $d_2 = 500$ nm. Granules subject to van der Waals force only, and subject also to an added capillary force or bonding force were considered. Note that the yield strengths of the granules are indicated on the corresponding estimation curves.

VI. Conclusion

A new synthesizing process and simulation of the particle-particle interaction dynamics of granules used to fabricate nano-Mo/Al₂O₃ composites powder have been presented. The results of simulation and characterization of the composite powder are summarized below.

- (1) The fluidization behavior of fine alumina powder is similar to that of soft granules with a broad size distribution due to the attractive forces. The interaction of the van der Waals force is important without considering the influence of capillary and atomic bonding when the surface distance is smaller than 1.0 nm. However, F_{vdW} is still a very weak force.
- (2) The simulation results show that the soft granules collide with a rigid boundary wall and subsequently form secondary granules in which size is a function of the impinging velocity and packing characteristics. The critical breakdown velocity of the hard granule with additional bonding forces is beyond the scope of the simulation.
- (3) The packing strength of the granule can be derived from the integration of three adhesive forces and from the surface distance between neighboring particles. The results of the experiment show the yield pressures of various granules to be similar, which is consistent with the results of numerical calculations.

- (4) The details of the morphologies obtained using TEM and SEM show that the Mo-species is homogeneously deposited on submicron alumina powder. The Mo-species diffuses into the interior spaces of the granules during fluidization, yielding Mo concentrations as high as 24 wt%.

Acknowledgment

The authors would like to acknowledge research funding provided by the National Science Council (NSC) of the Republic of China under contract NSC 88-2216-E-002-028 and by DAAD in Germany under a sandwich program.

References

- Bergstrom, L., A. Meurk, H. Arwin, and D. J. Rowcliffe (1996) Estimation of Hamaker constants of ceramic materials from optical data using Lifshitz theory. *J. Am. Ceram. Soc.*, **79**(2), 339-348.
- Bortzmeyer, D. (1997) Mechanical properties and attrition resistance of porous agglomerates. In: *Powder & Grains 97*, pp. 121-124. R.P. Behringer and J.T. Jenkins Eds. Balkema, Rotterdam, the Netherlands.
- Cheremisinoff, N. P. and P. N. Cheremisinoff (1986) *Hydrodynamics of Gas-Solid Fluidization*. Gulf Publishing Co. London, U.K.
- Cundall, P. A. (1971) A computer model for simulating progressive, large-scale movements in block rock systems. *Proceedings of the Symposium of the International Society of Rock Mechanics*, Vol. II, Art. 8, Nancy, France.
- Cundall, P. A. and O. D. L. Strack (1979) A discrete numerical model for granular assemblies. *Geotechnique*, **29**, 47-65.
- Geldart, D. (1973) Types of fluidization. *Powder Technol.*, **7**, 285-290.
- German, R. M. (1994) *Powder Metallurgy Science*, 2nd Ed. MPIF, Princeton, NJ, U.S.A.
- Hong, C. W. (1996) Discrete element modeling of colloidal packing dynamics during centrifugal casting. *J. Ceram. Soc. Jpn.*, **104**(9), 793-795.
- Hong, C. W. (1997) New concept for simulating particle packing in colloidal forming processes. *J. Am. Ceram. Soc.*, **80**(10), 2517-2524.
- Hong, C. W. (1998) From long-range interaction to solid-body contact between colloidal surfaces during forming. *J. Europ. Ceram. Soc.*, **18**, 2159-2167.
- Horn, R. G. (1990) Surface force and their action in ceramic materials. *J. Am. Ceram. Soc.*, **73**(5), 1117-1135.
- Hunter, R. J. (1987) *Foundations of Colloid Science*, Vol. 1. Oxford University Press, New York, NY, U.S.A.
- Kingery, W. D., H. K. Bowen, and D. R. Uhlmann (1976) *Introduction to Ceramics*, 2nd Ed. John Wiley & Sons, New York, NY, U.S.A.
- Kinemuchi, Y., T. Yanai, and K. Ishizaki (1996) In-situ formation of Si₃N₄-nano SiC composite. *Nanostruct. Mat.*, **9**, 23-32.
- Kwauk, M. (1992) Powder assessment. In: *Fluidization, Idealized and Bubbeless, with Applications*, Chap. 14, pp. 229-232. Ellis Horwood, New York, NY, U.S.A.
- Lander, J. J. and L. H. Germer (1947) Plating molybdenum, tungsten and chromium by thermal decomposition of their carbonyls. *Metal. Tech.*, **14**(6), 1-42.
- Lin, C. J., C. C. Yang, and W. J. Wei (2000) Processing and microstructure of nano-Mo/Al₂O₃ composites from MOCVD and fluidized bed. *NanoStructured Materials*, **11**(8), 1362-1377.
- Lo, M. H. and W. J. Wei (1997) Analysis of (Cr,Mo) oxycarbide films grown on stainless steel via metalloorganic chemical vapor deposition. *J. Am. Ceram. Soc.*, **80**(4), 886-892.
- Lok, Y. K. and T. C. Lee (1997) Processing of advanced ceramics using the wire-cut EDM process. *J. Mat. Pro. Tech.*, **63**, 839-843.
- Matsumoto, R. L. K. (1986) Generation of powder compaction response

- diagrams. *J. Am. Ceram. Soc.*, **69**(10), C246-C247.
- Nawa, M., T. Sekino, and K. Niihara (1994a) Improvement of fracture toughness of Al₂O₃/Mo nanocomposites. *J. Mat. Sci.*, **29**, 3185-3192.
- Nawa, M., K. Yamazaki, T. Sekino, and K. Niihara (1994b) A new type of nanocomposite in TZP-Mo system. *Mat. Letters.*, **20**, 299-304.
- Niihara, K. (1991) New design concept of structural ceramics – ceramic nanocomposites. *J. Ceram. Soc. Jpn.*, **99**(10), 947-982.
- Papargyris, A. D. (1998) Estimator type and population size for estimating the Weibull modulus in ceramics. *J. E. Ceram. Soc.*, **18**, 451-455.
- Rietema, K. (1991) *The Dynamics of Fine Powder*, pp. 152-157. Elsevier Applied Science, New York, NY, U.S.A.
- Roy, R., R. A. Roy, and D. M. Roy (1986) Alternative perspectives on quasi-crystallinity: Non-uniformity and nanocomposites. *Mater. Lett.*, **4**, 323-328.
- Szekely, J. J. W. Evans, and H. Y. Sohn (1976) *Gas-Solid Reactions*, Academic Press, New York, NY, U.S.A.
- Tsuji, Y. T. Kawaguchi, and T. Tanaka (1993) Discrete particle simulation of two-dimensional fluidized bed. *Powder Technology*, **77**, 79-87.
- Tsuji, Y. T. Tanaka, and S. Yonemura (1994) Particle induced turbulence. *Appl. Mech. Rev.*, **47**(6), part 2, 75-79.
- Walker, W. J. Jr. and J. S. Reed (1999) Influence of granule character on strength and Weibull modulus of sintered alumina. *J. Am. Ceram. Soc.*, **82**(1), 50-56.
- Wang, S. C. and W. J. Wei (1998) Microstructural development of Al₂O₃-composites with fine Mo particulates, II. Densification and mechanical properties. *NanoStructured Mat.*, **10**(6), 983-1000.
- Wei, W. J. and M. H. Lo (1998) Processing and properties of (Mo,Cr) oxycarbides from MOCVD. *Appl. Organometal. Chem.*, **12**, 201-220.
- Wei, W. J. S. C. Wang, and F. H. Cheng (1998) Microstructural development of Al₂O₃-composites with fine Mo particulates, I. Microstructural development. *NanoStructured Mat.*, **10**(6), 965-981.
- Wen, C. Y. and Y. H. Yu (1966) A generalized method for predicting the minimum fluidization velocity. *A. I. Ch. E. Jour.* **12**(3), 610-612.

以離散元素法模擬鉬／氧化鋁聚結在流體床中的行為及其製程研究

林慶章* 韋文誠* Takashi Iwai** 洪居萬** Peter Greil**

*國立臺灣大學材料科學與工程研究所

**德國阿朗根－紐倫堡大學材料科學系玻璃與陶瓷研究所

摘要

微細的氧化鋁陶瓷粉末由於數種作用力的作用而傾向形成聚結，藉由離散元素法 (Discrete Element Method, DEM) 來模擬粉末聚結中，顆粒與顆粒間在流體床中之動態交互作用。模擬結果顯示聚結團因為流體化而產生碰撞，軟聚結會在特定的碰撞速度及角度下破裂，而聚結強度和粉末聚結的堆積密度及粉末顆粒與顆粒間結合力的形態有關。模擬的結果並和四種不同密度的聚結強度及微結構的實驗結果相互比較。由製程所獲得的鉬／氧化鋁陶瓷複合粉體，藉由強度測試 (MTS)，掃描式電子顯微鏡 (SEM)，穿透式電子顯微鏡 (TEM) 及電子探測微分析儀 (EPMA) 的微結構觀察及分析顯示，模擬結果和實驗結果相當一致，微結構並顯示在有機金屬化學蒸鍍 (MOCVD) 流體床的製程中，鉬分子可以擴散進入次微米的聚結孔隙中，獲得均勻的金屬鉬／氧化鋁陶瓷複合粉體，其鉬含量高達24%重量比。